

Article

The Second Workshop on Lineshape Code Comparison: Isolated Lines

Spiros Alexiou ^{1,*}, Milan S. Dimitrijević ², Sylvie Sahal-Brechot ³, Evgeny Stambulchik ⁴, Bin Duan ⁵, Diego González-Herrero ⁶ and Marco A. Gigosos ⁶

¹ TETY, University of Crete, 71409 Heraklion, TK2208, Greece

² Astronomical Observatory, Volgina 7, Belgrade 11060, Serbia; E-Mail: mdimitrijevic@aob.rs

³ LERMA-UMR CNRS 8112 and UPMC, Observatoire Paris Meudon, 5 Pl Jules Janssen, Meudon 92195, France; E-Mail: sylvie.sahal-brechot@obspm.fr

⁴ Faculty of Physics, Weizmann Institute of Science, Rehovot 76100, Israel; E-Mail: evgeny.stambulchik@weizmann.ac.il

⁵ Institute of Applied Physics and Computation Mathematics, Beijing 100088, China; E-Mail: alexduan1967@hotmail.com

⁶ Departamento de Optica, Universidad de Valladolid, Valladolid 47071, Spain; E-Mails: diegohe@opt.uva.es (D.G.-H.); gigosos@coyanza.opt.cie.uva.es (M.A.G.)

* Author to whom correspondence should be addressed; E-Mail: moka1@otenet.gr; Tel.+306937545547.

Received: 14 March 2014; in revised form: 9 April 2014 / Accepted: 25 April 2014 /

Published: 12 May 2014

Abstract: In this work, we briefly summarize the theoretical aspects of isolated line broadening. We present and discuss test run comparisons from different participating lineshape codes for the 2s-2p transition for LiI, B III and NV.

Keywords: Stark broadening; isolated lines; impact approximation

1. The Importance of Level Spacings

In a plasma, free electrons and ions interact and perturb atomic states, resulting in line broadening and shift [1,2]. Each free plasma particle coming appreciably close to the emitter will contribute to the broadening and, in principle, also, the shift. This contribution will depend not only on the proximity of

the emitter and perturber, but also on the duration of the interaction, i.e., the time interval during which the interaction is appreciable. Isolated lines are lines where for the upper and lower levels, the closest perturbing level is energetically much further away than the inverse collision duration. For instance, for the 2s-2p lines considered, the 2s-level states are perturbed by the 2p states in the sense that the important broadening process is:

$$|2s\rangle \rightarrow (\text{via a collision}) |2p\rangle \rightarrow (\text{via a collision}) |2s\rangle \tag{1}$$

In general, we consider the broadening process:

$$|\alpha\rangle \rightarrow (\text{via a collision}) |\alpha'\rangle \rightarrow (\text{via a collision}) |\alpha\rangle \tag{2}$$

For isolated lines, the relevant energy spacings, $\omega_{\alpha\alpha'}$, between the collisionally connected states, α and α' , is of paramount importance. These energy spacings effectively reduce the interaction time and the effective impact parameters. For example, the relevant plasma-related quantity is, for perturbative collisions and a long-range dipole interaction [3]:

$$\phi = \frac{ne^2}{\hbar^2} \int_{-\infty}^{\infty} dt_1 \int_{-\infty}^{t_1} dt_2 \langle \mathbf{E}(t_1) \cdot \mathbf{E}(t_2) \rangle e^{i\omega_{\alpha\alpha'}(t_1-t_2)} \tag{3}$$

where

$$\langle \mathbf{E}(t_1) \cdot \mathbf{E}(t_2) \rangle = \frac{2\pi}{3} \int_0^{\infty} v f(v) dv \int_0^{\rho_{max}} \rho d\rho \mathbf{E}(t_1) \cdot \mathbf{E}(t_2) \tag{4}$$

Here, $\mathbf{E}(t)$ is the electric field at the emitter, due to the perturbing particle with impact parameter ρ and velocity (at an infinite distance from the emitter) v . We note the decreasing width with increasing temperature, e.g., $\frac{\ln T}{\sqrt{T}}$ [4]; the width is dominated by a $T^{-1/2}$ decay [5] for straight line trajectories.

The imaginary exponential has the following important effects compared to the collisionally degenerate (hydrogenic, $\omega_{\alpha\alpha'} = 0$) case:

1. Only a part of the collision duration is effective, i.e., the effective collision duration is shortened, not the entire collision.
2. Since the impact parameter affects the collision duration ($\propto \rho/v$), the effective impact parameters are also smaller.
3. The effective velocities increase (slow collisions are adiabatic).
4. As a corollary to all the above, broadening is decreased.

For strong collisions, we also have (canceling) higher order terms in the Dyson expansion. However, it is still true that the collision duration is effectively shortened by the imaginary exponentials.

In all calculations, only the 2s and 2p levels were considered. The only exception was the fully quantum-mechanical code [6], which used 13 nonrelativistic configurations $1s^2nl$ ($n = 2, 3, 4, 5, l \leq 4$) for B III and NV.

2. Electron vs. Ion Broadening

For hydrogen, given a velocity and impact parameter, a straight line trajectory gives the same contributions for any *single* electron and singly-charged ion.

For a hydrogen-like emitter, electrons are attracted; hence, they come closer, but also are accelerated, hence spending less time in the vicinity of the emitter. Ions are repelled, hence staying further away, but also slowing down; hence, they stay longer in the vicinity of the emitter. The action is $\int V(t)dt$, with $V(t)$ the emitter-perturber interaction; hence, the net effect is that the same velocity electron and singly charged ion contribute the same to broadening [3]. Of course, ion perturbers win overall, due to their velocity distribution favoring smaller velocities, both for hydrogen and hydrogen-like emitters.

For isolated lines, the action is $\int V(t)e^{i\omega_{\alpha\alpha'}t}dt$. Therefore, only times of the order $1/\omega_{\alpha\alpha'}$ contribute. For electrons, this is not too bad: electrons rely on coming close, and since they are accelerated, their effective collision duration is small anyway. For ions, however, the consequences are far greater: ions were kept away and relied on a longer duration interaction to match the electrons. Now that a longer duration is negated by the shrinking of the effective collision duration to $\propto 1/\omega_{\alpha\alpha'}$, the ions are ineffective [3].

The bottom line is that, for isolated lines, ions normally cannot compete with electrons, with two exceptions: (A) when $\omega_{\alpha\alpha'}$ is small compared to kT , in which case, the collision duration was very short anyway; (B) ions can compete in non-dipole interactions. In contrast to the dipole case, we can have the channel

$$|\alpha\rangle \xrightarrow{\text{via a quadrupole collision}} |\alpha\rangle \xrightarrow{\text{via another quadrupole collision}} |\alpha\rangle$$

as result of a quadrupole excitation/deexcitation. Non-dipole interactions are, however, outside the scope of the workshop comparison and were explicitly neglected in all calculations, except the fully quantal one.

As a result, isolated lines allow a test of electron broadening alone. For the calculations submitted to the workshop and considered in the present paper, ion broadening was explicitly neglected for both widths and shifts. The electron densities used were $n_e = 10^{17}$ e/cm³ for LiI, $n_e = 10^{18}$ e/cm³ for B III and $n_e = 10^{19}$ e/cm³ for NV. However, the results are presented, normalized to a density of 10^{17} e/cm³, that is, the B III results were divided by 10 and the NV results by 100.

3. Penetrating Collisions

These are collisions where the perturbing particle penetrates the emitter wavefunction extent for the states involved. As already discussed above, since smaller impact parameters gain in importance, penetration is more important for isolated lines:

For instance, for neutrals, the collision duration is $\propto \rho/v$, so that the impact parameters, ρ , and velocities, v , that contribute significantly are such that $\rho\omega_{\alpha\alpha'} \leq v$, e.g., small ρ . Hence, close collisions, which typically dominate for isolated lines, are significantly affected by penetration [7], which softens these collisions. This effect can be quite important and typically produces a factor of a two-width decrease [8].

Thus, if penetration is accounted for, perturbation theory is typically valid. This is convenient, since by softening the interaction, penetration makes those important close collisions perturbative; hence, much easier to solve. On the downside, there is no one-size fits all formula, i.e., instead of universal broadening functions, now we have per species and line broadening functions, although universal formulas that account for penetration have been given for hydrogen [10] and are possible for H-like ions. Furthermore, wavefunction information is needed, and oscillator strengths are no longer adequate [8].

4. Quantal Calculations

In contrast to semiclassical calculations, which assume the perturbing particles to be classical particles moving in well-defined trajectories, quantal calculations model the perturbing particles in terms of their wavefunctions and consider quantal effects, such as temporary electron capture and resonances. Only one fully quantal calculation participated in the workshop (DARC).

Fully quantal calculations have been performed by a number of different methods, e.g., Coulomb–Born (CB), distorted waves (DW), up to close coupling (CC) (R-matrix [11] and convergent close coupling (CCC) [12]). CB agreed very well with CC, which is understandable, due to the weakness of the interaction. Comparisons of quantal and semiclassical calculations have been done and summarized [8,13]. Good agreement is found if the penetration is taken into account in semiclassical calculations. What is puzzling is a recent DW calculation by Elabidi *et al.* [14] citing the agreement with the experiments; these results are a factor of two larger than the aforementioned CC calculations. The present K-matrix CC calculations of DARC also agree with experiments and show the factor of two disagreements with the previous CC calculations. It is not clear why the DW [14] and DARC show such a large difference with R-matrix and CCC.

4.1. Work to be Done on Quantal Calculations

This is an open issue, and work is needed to pinpoint the origin of these differences. Comparing partial wave results and/or cross-sections may be helpful. We have not resolved the discrepancy with experiments. A code comparison may be needed to assess the relative importance of various factors in quantal calculations.

4.2. Work to be Done with Semiclassical Calculations

If penetration and non-perturbative aspects are accounted for, the remaining differences between the quantal and semiclassical approach are due to [8,13]:

- a. The demarcation line between what may and what may not be treated semiclassically.
- b. Back-reaction issues, i.e., in classical terminology, deviations from the (straight line or hyperbolic) trajectory, due to the energy transfer between the perturber and emitter; e.g., for collisional excitation/deexcitation, in our case, between the 2s and 2p levels, given that these energy transfers are comparable to the thermal velocities.

Answers to these questions may be given by Feynman path calculations. Such calculations have started appearing, but only for the simplest cases [15].

5. (Dynamic) Shifts

Shifts are caused by the finite collision duration. The same considerations apply as for widths: Ion (dipole) shifts are typically negligible; penetration is also an important factor. In contrast to widths, where one is looking for the guaranteed nonnegative deviation of $Re(I - S_a S_b^*)$ of a quantity, possibly small, from unity, with shifts, one is looking for the deviation of a possibly small quantity, $Im(I - S_a S_b^*)$ from zero. Furthermore, canceling opposite sign contributions arise [16], and the end result is that a small error in the calculation or deviation from thermal distribution functions can change the shift sign. This study was repeated [17] and confirmed the results for $\Delta n = 0$, but found consistent red shifts for $\Delta n \neq 0$. The recommendation of [17] is that $\Delta n \neq 0$ shifts are reliable, while $\Delta n = 0$ are not.

6. The Codes

Three types of codes participated in the workshop: DARC [6], a fully quantal (K-matrix) close-coupling code that, in principle, should be the benchmark, but uses a different physical model from the rest, full simulation codes (SimU [18] and Simulation [19]), which, in principle, may also account for perturber–perturber interactions, though for the cases presented in this comparison, perturbing electrons were modeled as non-interacting quasiparticles interacting with the emitter via Debye-shielded fields and semiclassical impact codes (SCP [20–23], a perturbative impact code and Starcode [8]). Starcode is a non-perturbative impact code, which solves the Schrödinger equation if it considers that the perturbative calculation has too large calculation uncertainties (and with the current tolerance, it invariably does). Although Starcode is a single code, it has a number of options, and in the present paper, we refer to two Starcode versions: one version, referred to as Starcode, which accounts for penetrating collisions, and one, called Starcode-NP, which does not. In practice, this is controlled by a single option in the input file.

The problem specification was that only dipole electron broadening should be considered. Except for DARC, which includes non-dipole interactions, all other codes have adhered, either by default or by selection of the appropriate options, to this specification. However, judging from Starcode calculations with monopoles and quadrupoles, the inclusion of monopole and quadrupole interactions makes too small a difference to explain the differences with DARC. Previous quantal close-coupling calculations have also produced widths that are a factor of two smaller than the ones quoted by DARC, as discussed above.

In addition, the problem specifications were to neglect fine structure, but only the simulation codes adhered to this specification. Among the codes, only SimU uses a Debye-shielded electron-emitter interaction, while all others use either a pure Coulomb interaction (DARC, Simulation) or a cutoff length of the order of the Debye length. In view of the remarks on short impact parameters being most important, these differences are not expected to be significant. For example, for SimU, the difference in the calculations using pure Coulomb or Debye-shielded fields is of the order of 0.1%. Small differences when using Coulomb or Debye-shielded fields have also been confirmed in tests using Simulation.

Atomic data are discussed in the Appendix.

7. Strong Collisions

The term “strong collisions” has been used in the literature to denote either “collisions that may not be treated by perturbation theory” or “collisions that may not be treated within the model used”, e.g., collisions for which the semiclassical approximation is not valid or collisions for which the normally employed long-range approximation is not valid. Note that the two definitions may be in conflict. For example, penetrating collisions may be non-perturbative within the long-range approximation and perturbative if the long-range approximation is not used. Impact codes SCP and Starcode use the second definition and estimate the strong collision contribution based on unitarity. Starcode, which is non-perturbative, actually computes the non-perturbative contribution exactly within the impact approximation, but excludes from the computation the phase space for which its model is physically not valid. Simulation and SimU make no distinction between strong and weak collisions, as they are treated in exactly the same way. The simulation codes compute strong collisions (even if the model used is physically invalid due to quantal effects and/or the long-range dipole approximation), as well as weak ones. However, we consider simulation codes to employ the first definition when we wish to consider the differences between simulation codes and perturbative results. Hence, in principle, differences between the simulation codes and Starcode-NP should be due to either non-impact (overlapping) collisions or the phase space part that is excluded from Starcode and included in the simulation. For DARC, this distinction is rather meaningless.

Generally speaking, good agreement is expected between all codes for the non-strong (in either meaning) contributions, while things are not as clear for strong collisions in either meaning.

8. Computational Uncertainties

With respect to calculational uncertainties, the codes use quite different ways of estimating them.

- DARC. Calculation uncertainties were estimated by increasing the orbital angular momentum of the colliding electron up to 25. They turned out to be $\ll 5\%$ [6].
- SCP. For simple spectra, an error bar of 20% was adopted, based on the average agreement with the experimental results for He I lines [24] and Si-like ions [25], namely 17% for widths and 20% for shifts.
- SimU. This is a full simulation code that computes the line profile directly instead of first computing the autocorrelation function. It is a semiclassical, long-range dipole code that handles non-perturbative aspects, as well as non-impact effects rigorously. SimU calculates $|\vec{D}(\omega)|^2$, where $\vec{D}(t)$ is the dipole operator and $\vec{D}(\omega)$ is its Fourier transform. The procedure is repeated N times ($N \gg 1$) and averaged, which corresponds to an averaging over a statistically representative ensemble of radiators. The uncertainty due to a finite statistical sampling is $\propto 1/\sqrt{N}$, and the proportionality coefficient is inferred by observing convergence over the course of simulations. For details, see [26]. Another important factor affecting the calculational accuracy is the finite step of the frequency grid, equal to t_{\max}^{-1} , where t_{\max} is the time over which $\vec{D}(t)$ is calculated in each run prior to averaging. Contrary to the first (statistical) factor, the latter always results in an

overestimate of the line width by $\sim t_{\max}^{-1}$. For the shift values, this factor contributes $\pm \sim t_{\max}^{-1}/2$. The total uncertainties were within 10% for the cases considered.

- Simulation. The spectra is obtained through a Fourier transform of the autocorrelation function, which has been obtained by computer simulation and averaged over a large enough number of samples. The error is estimated using several sets of configurations to average the autocorrelation function and comparing the results obtained in each case. These fluctuations are about 3% using sets of 10,000 runs.
- Starcode. Starcode has two sources of errors: numerical errors, e.g., from integrations or solutions of the Schrödinger equation, which are controlled through appropriate tolerances and are generally negligible, and errors arising from the model used, which are the ones quoted here. Starcode recognizes that there is a part of the phase space for which the model used (e.g., semiclassical trajectories and, in the version without penetration, trajectories that penetrate the wavefunction extent) is not reliable. However, the contribution of that part of the phase space may be bound by unitarity. Thus, one first defines $v_0 = \frac{\hbar}{m\rho_{\max}}$. This is a velocity below which all collisions have a de Broglie wavelength larger than the screening length, ρ_{\max} , and, hence, are definitely non-classical. The corresponding phase space makes a contribution:

$$E_1 = 2\pi n \int_0^{v_0} v f(v) dv \int_0^{\rho_{\max}} \rho d\rho \operatorname{Re}[I - S_a(\rho, v) S_b^*(\rho, v)] \quad (5)$$

$$= \pi n \alpha \sqrt{\frac{8m}{\pi kT}} \rho_{\max}^2 (1 - (1 + w_0) e^{-w_0})$$

with n the electron density, $f(v)$ the velocity distribution, S_a and S_b the S-matrices for the upper and lower levels, respectively, $w_0 = \frac{mv_0^2}{2kT}$ and α is an estimate for the average $\operatorname{Re}[I - S_a(\rho, v) S_b^*(\rho, v)]$, which is between zero and two, due to unitarity. In practice, this contribution is negligible in our examples.

For $v > v_0$, the semiclassical approach is not valid for $\rho < \frac{b\hbar}{mv}$, where b is a parameter, taken to be one in the present calculations, which specifies how much larger than the de Broglie wavelength an impact parameter must be in order to be treatable semiclassically. Hence, if penetration is allowed, this non-semiclassical phase space provides the dominant contribution:

$$E_2 = 2\pi n \int_{v_0}^{\infty} v f(v) dv \int_0^{\frac{b\hbar}{mv}} \rho d\rho \operatorname{Re}[I - S_a(\rho, v) S_b^*(\rho, v)] = 2\pi n \alpha \left(\frac{b\hbar}{m}\right)^2 \sqrt{\frac{2m}{\pi kT}} e^{-w_0} \quad (6)$$

If penetration is not allowed, then the upper limit of the ρ integral is $\max(R, \frac{b\hbar}{mv})$ with R the relevant wavefunction extent, e.g., the maximum spatial extent of the 2s and 2p levels in our case. Hence, E_2 in the case with penetration is replaced by $E_{2NP} + E_3$ with:

$$E_{2NP} = 2\pi n \int_{v_0}^{v_1} v f(v) dv \int_0^{\frac{b\hbar}{mv}} \rho d\rho \operatorname{Re}[I - S_a(\rho, v) S_b^*(\rho, v)] \quad (7)$$

$$= 2\pi n \alpha \left(\frac{b\hbar}{m}\right)^2 \sqrt{\frac{2m}{\pi kT}} (e^{-w_0} - e^{-w_1})$$

with $v_1 = \frac{\hbar}{mR}$ and $w_1 = \frac{mv_1^2}{2kT}$ and

$$E_3 = 2\pi n \int_{v_1}^{\infty} v f(v) dv \int_0^R \rho d\rho \operatorname{Re}[I - S_a(\rho, v) S_b^*(\rho, v)] = \pi n \alpha \sqrt{\frac{8m}{\pi kT}} R^2 (1 + w_1) e^{-w_1} \quad (8)$$

This ensures that, provided one trusts the choices of b and R , only truly semiclassical paths are computed, and a rigorous, unitarity-based error bar may be returned for the part of the phase space that is not treatable semiclassically. Of course, other sources of error, e.g., the back reaction, are not accounted for.

For the cases treated here with penetration not allowed, the wavefunction extent was dominant for all temperatures in the LiI calculations, for $T = 15$ and 50 eV for B III and $T = 50$ eV for NV. The de Broglie cutoff was dominant for the remaining cases. Hence, if the de Broglie cutoff is dominant, the Starcode and Starcode-NP calculations should have the same error bar, and Starcode-NP should have a larger width, due to the stronger interaction. If R is the dominant cutoff, then the error bar of Starcode-NP should be significantly larger and the computed width of Starcode might even exceed (with the error bar not accounted for) Starcode-NP, due to the larger phase space that is contributing. Of course, the situation will be reversed when the calculation uncertainties are accounted for. Width results are quoted as (the width from the part of phase space that is computed reliably $+\frac{1}{2}$ error bar) $\pm\frac{1}{2}$ error bar. Shifts are quoted as (the shift from the part of phase space that is computed reliably) \pm error bar. All Starcode and Starcode-NP strong collision estimates assume a constant $Re(I - S_a S_b^*) = 1$ for that part of the phase space.

9. Results: Widths

Widths are shown in Table 1. All widths have been normalized to a density of 10^{17} e/cm³.

Table 1. 2s-2p Transition width (FWHM) comparisons. All widths are in cm⁻¹ and normalized to a density of 10^{17} e/cm³.

Species	T (eV)	Model	DARC	SCP	SimU	Simulation	Starcode-NP	Starcode
LiI	5	straight		1.05	0.82	0.88	0.95	0.84
LiI	15	straight		1.10	0.87	0.96	0.87	0.72
LiI	50	straight		1.00	1.08	0.88	0.80	0.51
B III	5	hyperbolic	0.322	0.33	0.2		0.3	0.2
B III	5	straight		0.15	0.112	0.114		
B III	15	hyperbolic	0.259	0.207	0.173		0.2	0.13
B III	15	straight		0.139	0.128	0.128		
B III	50	hyperbolic	0.187	0.138	0.136		0.15	0.092
B III	50	straight		0.126	0.13	0.122		
NV	5	hyperbolic	0.199	0.197	0.1135		0.133	0.088
NV	5	straight		0.071	0.015	0.043		
NV	15	hyperbolic	0.1228	0.117	0.08		0.084	0.056
NV	15	straight		0.0535	0.0488	0.0487		
NV	50	hyperbolic	0.0812	0.07	0.0584		0.06	0.036
NV	50	straight		0.0476	0.044	0.0469		

9.1. General Remarks

1. In general, hyperbolic path calculations produced broader lines than straight line paths. This is expected, because due to the energy spacings (imaginary exponentials), only times closest to the time of the closest approach ($t = 0$) are important, but for these times, the electron is closer to the emitter if it is moving in a hyperbolic rather than a straight line path. Hence, the interaction is stronger, which results in larger widths.
2. Non-perturbative collisions (impact or not) are treated correctly in simulations and by strong collision or error estimates in perturbative impact codes. This is not an issue for non-perturbative impact codes. Non-perturbative collisions are significant if penetration is not accounted for.
3. Furthermore, in all cases, Starcode (with penetration) produces the lowest widths. This, however, is understood and expected, as Starcode with the option in question uses a different physical model that accounts for penetration, which, in turn, softens the interaction and results in smaller widths.
4. DARC consistently produces large widths, in many cases, more than twice the results of Starcode, which also accounts for penetrating collisions. This is not understood and at variance with previous fully quantum mechanical close-coupling calculations, as discussed above.
5. When investigating the differences between impact codes and simulations, particularly at low temperatures, one should keep in mind that impact codes treat all particles as impacting, while with simulation codes, the slow particles that are not impacting are treated correctly, i.e., differences could arise from non-impact effects for some particles. This would, in principle, mean lower widths for the simulations and should be less of an issue, at least for non-perturbative calculations at higher T . If that is correct, agreement should improve with non-perturbative impact calculations at higher T . As shown below, this is indeed the case for B III and NV, while the opposite is true for LiI. Note, however, that quantitatively non-impact effects are not expected to be an issue, as discussed below.
6. Another issue is the temperature dependence, where we find some codes and cases with an increasing width with increasing temperature or a width that varies very little with temperature. Intuitively, one might expect that higher temperatures mean weaker collisions and, hence, smaller widths. We know, however, that an increase in temperature sometimes actually results in larger widths, e.g., for initially strong collisions, such as non-impact ions [27].

Summing up, a non-decreasing temperature behavior, as observed in the simulation codes, may be the result of either non-impact effects or a significant or dominant strong collision term. The first possibility seems unlikely from simple estimates, discussed below, while if non-impact effects were negligible and the second were the case, then, since Starcode-NP is also a non-perturbative impact code, the differences from Starcode-NP would be due to the non-semiclassical phase space, as well as the emitter relevant wavefunction extent. This would have to be significant enough to change the widths *vs.* the temperature behavior. To check this conjecture, we list in Table 2 the Starcode-NP width contributions from the phase space part where Starcode-NP is presumably valid (labeled “non-strong” in Table 2, even though it includes non-perturbative collisions), as well as the “strong” collision contribution from the non-semiclassical and wavefunction extent phase space, where Starcode-NP (or any other workshop code, except DARC) is not valid. The actual

width quoted is as described above, e.g., $0.83 + 0.23/2 \pm 0.23/2$ for the lowest LiI temperature.

Table 2. 2s-2p Transition width (FWHM) strong collision importance in Starcode-NP. All widths are in cm^{-1} and normalized to a density of 10^{17} e/cm^3 .

Species	T (eV)	Starcode-NP Non-Strong	Starcode-NP Strong
LiI	5	0.83	0.23
LiI	15	0.69	0.39
LiI	50	0.48	0.7
B III	5	0.286	0.042
B III	15	0.172	0.048
B III	50	0.11	0.078
NV	5	0.114	0.038
NV	15	0.072	0.025
NV	50	0.0454	0.03

Therefore, we conclude that the differences between Starcode-NP and the simulation codes, as well as the different temperature trends exhibited are within the calculation uncertainties.

9.2. LiI Results

Figure 1 displays the results from five codes. Interestingly, only Starcode, in both versions, displays a decreasing width with temperature behavior (Within the semiclassical model, threshold issues do not arise, as we have virtual excitations and deexcitations, and a higher T means weaker interactions, due to their shorter duration.) All three other calculations produce an increase in the width as T rises from five to 15 eV. Simulation varies very little with temperature. With SimU, that trend continues out to $T = 50$ eV, whereas for SCP and Simulation, it is reversed. For SCP, this may be attributed to the symmetrization, which respects the quantum properties of the S-matrix rather than the method of computing the strong collision term, which is less than half the width already at 5 eV and decreases with T . For simulations, a possible explanation would be a non-impact behavior for electrons at low T . However, simple estimates do not support this conjecture. For example, at $T = 1$ eV, $n = 10^{17} \text{ e/cm}^3$ and $L - \alpha$, electrons are well impacted [28], and it is hard to see why they would be non-impacted at 5 eV for Li with a longer lifetime (inverse HWHM), due to the smaller matrix elements and imaginary exponentials. Hence, the most likely origin is [27], the increasing width vs. temperature for strong collisions. As already discussed, however, within the calculational uncertainties, Starcode-NP could also be made to show an increasing width with temperature.

9.3. B III Results

Figure 2 displays the widths from five codes. General trends are confirmed, with DARC giving the largest widths. SCP and Starcode-NP exhibit fairly good agreement, but the disagreement of SimU with Starcode-NP and the agreement of SimU with Starcode at low T (which is not expected, as SimU does not account for penetrating collisions, which make the difference between Starcode and Starcode-NP) and Starcode-NP at high T (which is expected) is puzzling. As shown in Table 2, the non-strong Starcode-NP

contribution alone is significantly larger than SimU’s total width, and the strong contribution will only increase the width of Starcode-NP and, hence, the difference.

Figure 1. A comparison of LiI 2s-2p transition widths as computed by SCP (solid black), SimU (dotted red), Simulation (dashed green) and Starcode with (dash-dotted blue) and without (dash-double dotted orange) penetration accounted for.

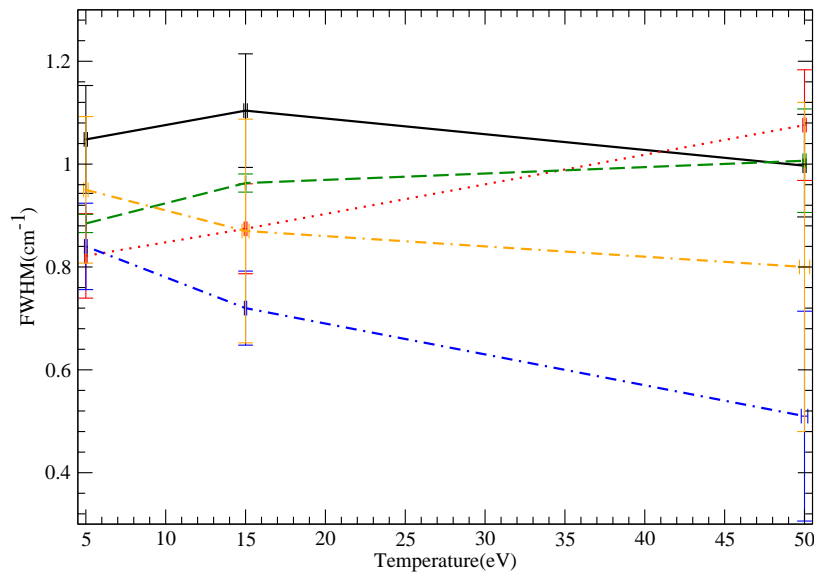


Figure 2. A comparison of hyperbolic trajectory B III 2s-2p transition widths as computed by SCP (solid black), SimU (dotted red), DARC (dashed green) and Starcode with (dash-dotted blue) and without (dot-double dash orange) penetration accounted for.

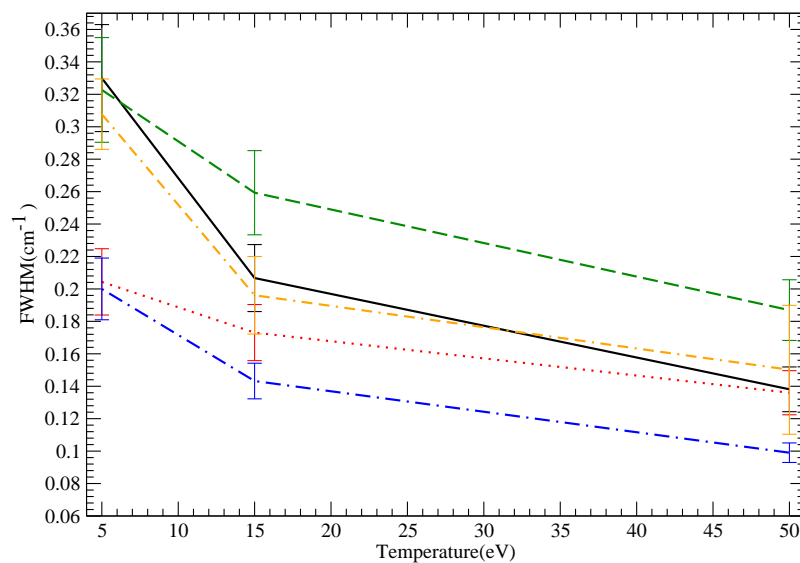


Figure 3 compares straight and hyperbolic trajectory results where applicable. Overall, the comparison demonstrates the difference, particularly for SCP, that arises from including vs. neglecting the attraction by the emitter. One would have expected a closer agreement between SimU and Simulation,

which use the same physical model. For SimU and Simulation, we see a width increase with increasing T , as already discussed. This increase is reversed for Simulation, but not for SimU. At high T , the calculations converge, as expected.

9.4. NV Results

Figure 4 displays the widths from five codes. SimU and Starcode-NP agree quite well, which is expected, at least for high temperatures, where non-impact effects should play no role. SCP and DARC also agree quite well with each other; however, their disagreement with other codes at the highest T value is not understood, since close coupling effects are expected to be negligible at this high T . All codes show the expected decrease for the widths as a function of T , as collisions weaken with increasing emitter charge Z [25].

Figure 5 compares straight and hyperbolic trajectory results, where applicable. Overall, the comparison demonstrates the significant difference that arises from including vs. neglecting the attraction by the emitter. Due to the higher Z , it is expected that these differences would be more pronounced than the differences found for B III. The close agreement of SimU-straight and Simulation-straight is expected, as both codes use the same physical model.

Figure 3. A comparison of hyperbolic and straight line trajectories for the NV 2s-2p transition widths, as computed by SCP-hyperbolic (solid black), SCP-straight (dotted red), SimU-hyperbolic (dashed green), SimU-straight (dash-dotted blue) and Simulation (dash-double dotted orange).

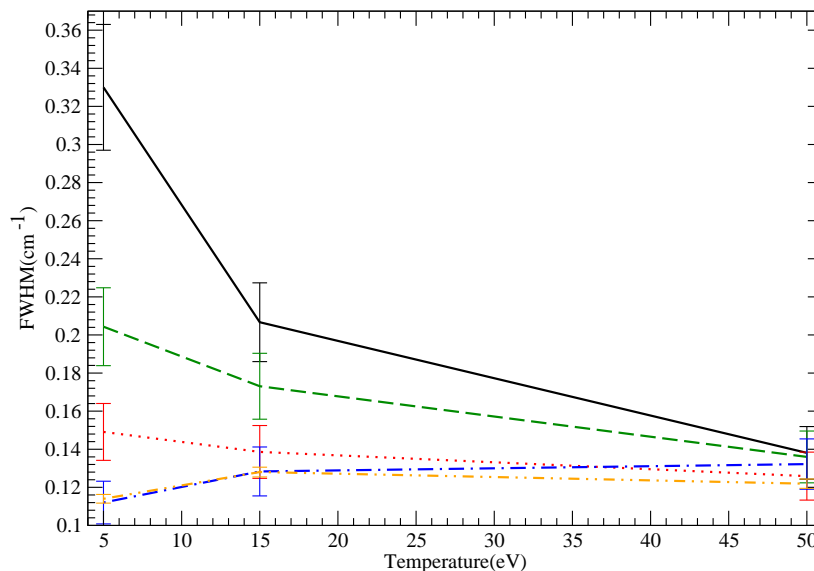


Figure 4. A comparison of hyperbolic trajectory NV 2s-2p transition widths, as computed by SCP (solid black), SimU (dotted red), DARC (dashed green) and Starcode with (dash-dotted blue) and without (dot-double dash orange) penetration accounted for.

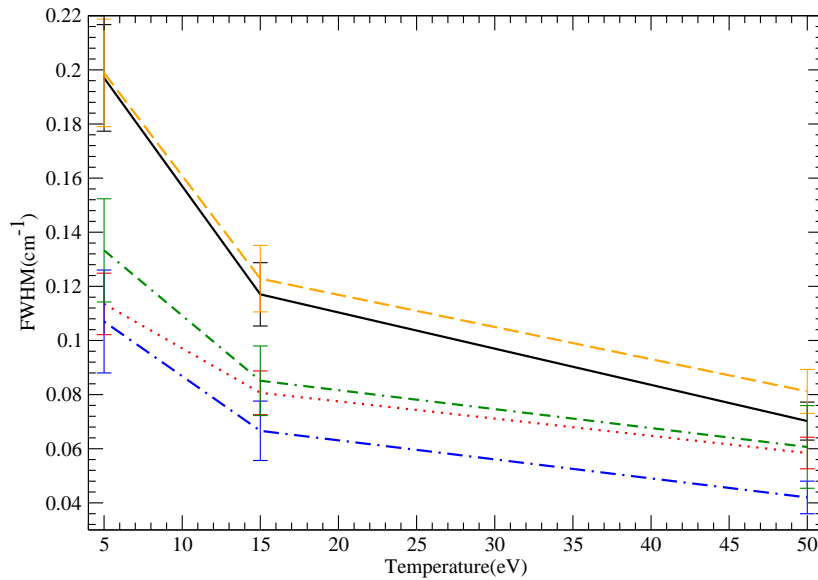
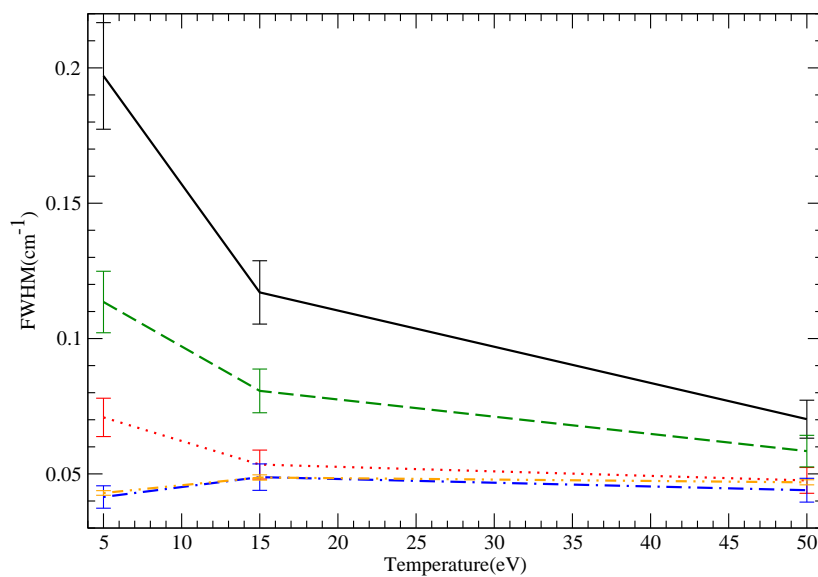


Figure 5. A comparison of hyperbolic and straight line trajectories for the NV 2s-2p transition widths, as computed by SCP-hyperbolic (solid black), SCP-straight (dotted red), SimU-hyperbolic (dashed green), SimU-straight (dash-dotted blue) and Simulation (dash-double dotted orange).



10. Results: Shifts

As discussed, shift calculations within the stated case definitions are probably inaccurate, but the comparisons may well illustrate trends and code differences. The results are summarized in Table 3. Shifts were normalized to a density of 10^{17} e/cm³.

Table 3. 2s-2p Transition shift comparisons of all shifts are in cm⁻¹ and normalized to a density of 10^{17} e/cm³.

Species	<i>T</i> (eV)	Model	DARC	SCP	SimU	Simulation	Starcode-NP	Starcode
LiI	5	straight		0.551	0.498	0.457	0.21	0.2
LiI	15	straight		0.42	0.43	0.368	0.29	0.28
LiI	50	straight		0.271	0.282	0.247	0.29	0.27
B III	5	hyperbolic	0.085	0.024	0.0846		0.05	0.063
B III	5	straight		0.0751	0.065	0.062		
B III	15	hyperbolic	0.058	0.0276	0.051		0.04	0.044
B III	15	straight		0.0606	0.0515	0.0515		
B III	50	hyperbolic	0.0265	0.0241	0.0363		0.03	0.03
B III	50	straight		0.0398	0.0352	0.0355		
NV	5	hyperbolic	0.0694	0.00423	0.031		1	2
NV	5	straight		0.0284	0.0222	0.02375		
NV	15	hyperbolic	0.03796	0.0054	0.0183		0.009	0.014
NV	15	straight		0.0233	0.0199	0.0199		
NV	50	hyperbolic	0.01776	0.0065	0.01275		.008	0.01
NV	50	straight		0.01535	0.0138	0.01355		

10.1. General Remarks

1. In general, we expect that if shifts are perturbative, they should also decrease with increasing *T*, due to the weakening of the interaction. For the same reason, we expect a convergence of the straight line and hyperbolic trajectory results as $T \rightarrow \infty$. No such statement of decreasing shifts with increasing *T* can be made with certainty in the non-perturbative case.
2. Starcode, in particular (with or without penetration), often shows a very weak increase of shift with *T*, even in the version with penetration accounted for, which results in weak, perturbative collisions. The reason is that Starcode explicitly excludes the non-semiclassical phase space, e.g., impact parameters shorter than the de Broglie wavelength. (In addition, Starcode, without accounting for penetration, also excludes impact parameters inside the wavefunction extent, because, again, these may not be treated within a long-range approximation). When *T* decreases, this phase space, which may not be computed within the code's semiclassical framework, increases. Hence, the phase space that gives a shift that may presumably be reliably computed shrinks, while the phase space that may not be treated grows. For both shifts and widths, Starcode binds the contribution of the non-semiclassical phase space by unitarity and returns it as an error bar. Therefore, while the quoted shift may be fairly insensitive to *T*, the error bar is not. These results are to be interpreted as an uncertainty in shift calculations inherent in semiclassical calculations, i.e., the part of the phase

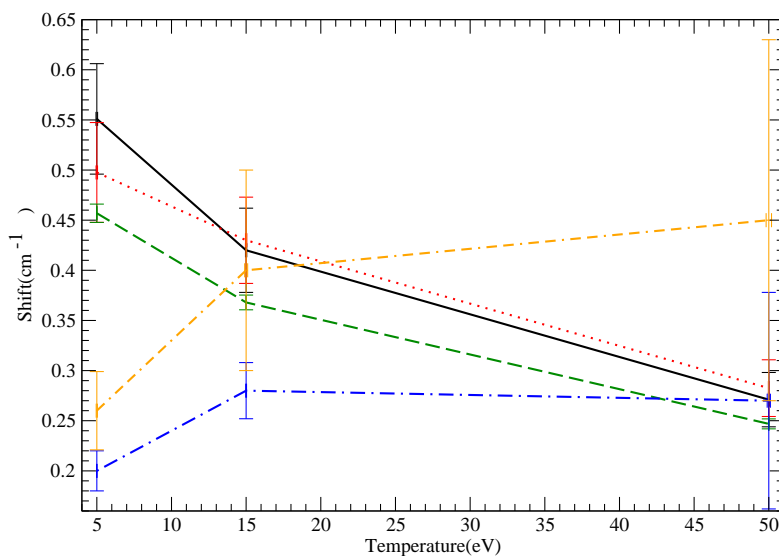
space that may not be treated semiclassically can make a substantial shift contribution rather than a temperature-insensitive shift.

3. Straight line SimU and Simulation agreement is excellent for the charged cases (B III and NV), as expected and, surprisingly, much poorer (though still good) for LiI.
4. SCP consistently gives significantly smaller shifts for ion lines (B III and NV). Furthermore, straight-line SCP calculations give significantly larger shifts than hyperbolic path SCP calculations. This is counterintuitive, since as discussed, hyperbolic paths result in a stronger effective interaction close to the emitter and, hence, action. Furthermore, the straight-line SCP shifts are monotonically decreasing as a function of T , in contrast to the hyperbolic trajectory results. This behavior follows the semiclassical b -functions [2], which result in lower shifts for hyperbolic compared to straight-line paths and, in addition, a decreasing b -function with increasing ion charge.

10.2. LiI

Figure 6 plots the shifts computed by five codes vs. electron temperature T . Except for Starcode (explained above), in both versions, the shift is decreasing with T , which is expected in view of the weakening of the interaction. The differences between the other three codes are generally better than 20%, although it is not clear why SimU and Simulation, which essentially use the same model and, hence, would, in principle, be expected to give the same results, differ by that amount.

Figure 6. A comparison of LiI 2s-2p transition shifts as computed by SCP (solid black), SimU (dotted red), Simulation (dashed green) and Starcode with (dash-dotted blue) and without (dot-double dash orange) penetration accounted for.



10.3. B III

Figure 7 plots the shifts computed by five codes vs. electron temperature T . The general trend (shifts decreasing with T) is observed, with the exception of the non-penetrative Starcode, which gives identical (within errors) results for the 15 and 50 eV cases, which has been discussed above, and SCP, which

shows a small increase between five and 15 eV. SCP is significantly lower for small T , which might be attributable to the use of perturbative impact theory by SCP, as it reflects the behavior of the semiclassical b -function. This is consistent with the convergence seen for higher T .

Figure 7. A comparison of B III 2s-2p transition shifts as computed by SCP (solid black), SimU (dotted red), DARC (dashed green) and Starcode with (dash-dotted blue) and without (dot-double dash orange) penetration accounted for.

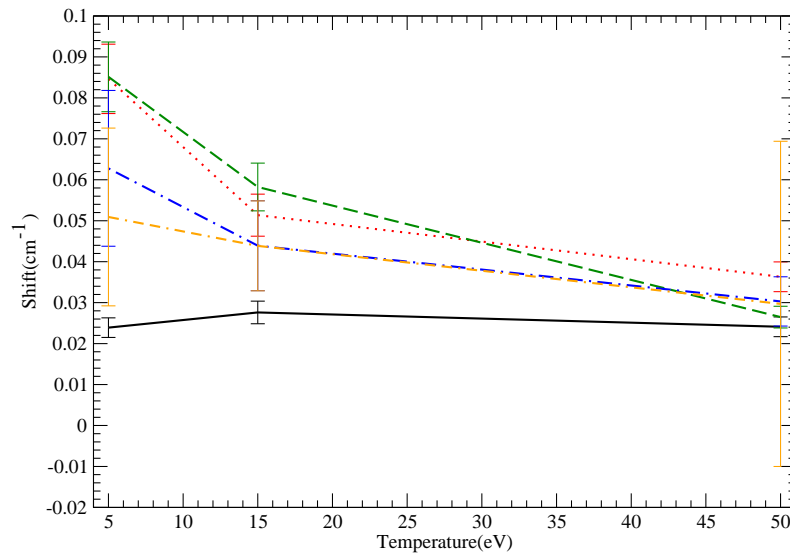


Figure 8. A comparison of hyperbolic and straight-line trajectories for the B III 2s-2p transition widths, as computed by SCP-hyperbolic (solid black), SCP-straight (dotted red), SimU-hyperbolic (dashed green), SimU-straight (dash-dotted blue) and Simulation (dash-double dotted orange).

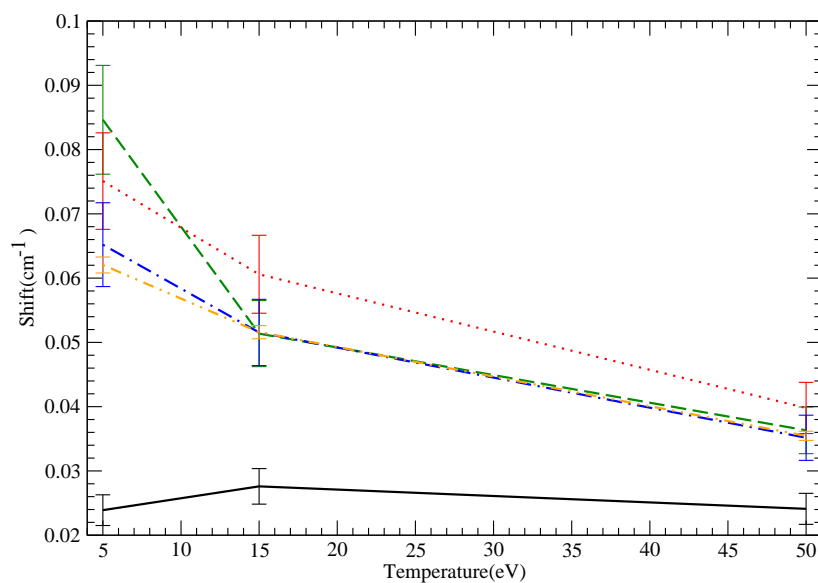


Figure 8 plots the shifts computed by five codes vs. electron temperature T . The straight line SimU and Simulation agreement is very good, as discussed above. The SimU hyperbolic trajectory shifts are

also in very good agreement with the mentioned straight-line results, except at the lowest T . SCP is also in fair agreement.

10.4. NV

Figure 9 plots the shifts computed by five codes vs. electron temperature T . DARC produces significantly larger shifts at low T , with all codes converging for large T . The large difference with Starcode seems to indicate that higher order partial waves (except the s-wave, which is viewed as an error bar in Starcode) differ substantially from the semiclassical results. SCP is lowest and exhibits insensitivity to T . SimU and Starcode without penetration also agree quite well, except at the lowest T . The lowest temperature point discrepancy between SimU and Starcode-NP could be due to the fact that Starcode does not compute the short impact parameter ($\rho < \frac{\hbar}{mv}$) contribution, which is not semiclassical, but adds an estimate to the shift, as discussed above. The calculations agree within their respective calculation uncertainties, although one might have expected a better agreement. However, attributing the difference to the phase space not included in the Starcode-NP calculation (but added as an error bar) does not seem to hold: For example, as already discussed, Starcode-NP calculations treat collisions with impact parameters larger than the de Broglie wavelength and use a unitarity-based estimate for smaller impact parameters. If instead, Starcode-NP treats all collisions with impact parameters larger than 0.1 times the de Broglie wavelength and only uses unitarity estimates for impact parameters smaller than 0.1 times the de Broglie wavelength, the shift actually decreases and is in the range of $1 = 1.5 \text{ cm}^{-1}$ at the lowest temperature, compared to a value of 3 cm^{-1} for SimU.

Figure 9. A comparison of NV 2s-2p transition shifts as computed by SCP (solid black), SimU (dotted red), DARC (dashed green) and Starcode with (dash-dotted blue) and without (dot-double dash orange) penetration accounted for.

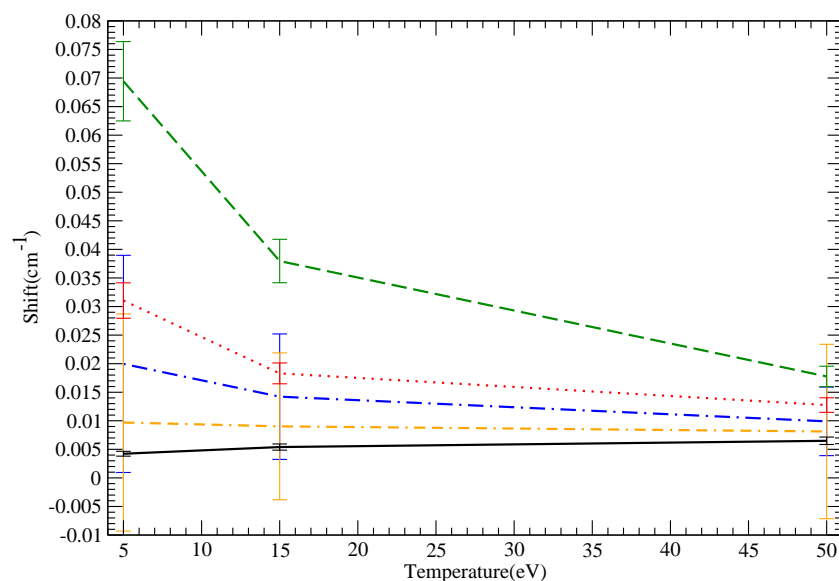
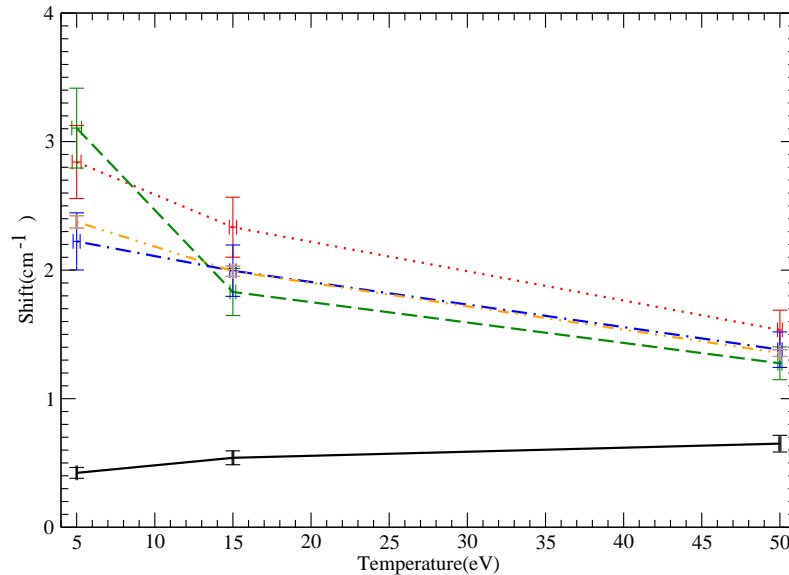


Figure 10 plots the shifts computed by five codes vs. electron temperature T .

Figure 10. A comparison of hyperbolic and straight line trajectories for the NV 2s-2p transition widths, as computed by SCP-hyperbolic (solid), SCP-straight (dotted), SimU-hyperbolic (dashed), SimU-straight (dash-dotted) and Simulation (dash-double dotted).



The three straight line results are in fairly good agreement, with SimU and Simulation being in excellent agreement. The hyperbolic trajectory and straight line SimU results are interesting in that the hyperbolic trajectory shift is larger at the lowest T (expected, as discussed in view of the stronger effective interaction for hyperbolic rather than straight line trajectories) and slightly smaller for the other two T values; however, that difference is within the calculation uncertainties, and the two calculations converge, as expected, for high T .

Acknowledgments

The authors would like to acknowledge the International Atomic Energy Agency (B.J. Braams and H.-K. Chung) for the organizational and financial support of this workshop.

Author Contributions

The present work is based on codes developed by all authors, who also participated in all aspects of this work.

Appendix A: Atomic Data

Atomic data were taken from the problem specification, with the 2s state taken as zero energy:

Table A1. 2s-2p Atomic Data.

Species	2p Energy (cm ⁻¹)	Oscillator Strength
LiI	14,903.89	0.7472
B III	48,381.07	0.3629
NV	80,635.67	0.234

Energies were averaged over fine structure components for $l > 0$, while reduced matrix elements were obtained from the respective multiplet-averaged oscillator strengths, f , via the equation:

$$|(nl|r|n'l')| = (-1)^{l+l'} \sqrt{\frac{3f(2l'+1)}{2(E_{nl} - E_{n'l'})}} \quad (9)$$

with $l_{>} = \max(l, l')$, i.e., one in our case.

Not all codes adhered to this specification. DARC, SCP and Starcode included fine structure and matrix elements used from atomic structure packages, as well as energies from these packages or experimental ones. However, in all cases, no significant differences were introduced in either the energy differences or the reduced matrix elements.

Conflicts of Interest

The authors declare no conflict of interest.

References

1. Griem, H.R. *Plasma Spectroscopy*; McGraw-Hill: New York, NY, USA, 1964.
2. Griem, H.R. *Spectral Line Broadening by Plasmas*; Academic: New York, NY, USA, 1974.
3. Alexiou, S. Collision operator for isolated ion lines in the standard Stark-broadening theory with applications to the Z scaling in the Li isoelectronic series 3P-3S transition. *Phys. Rev. A* **1994**, *49*, 106–119.
4. Elabidi, H.; Sahal-Brechot, S. Checking the dependence on the upper level ionization potential of electron impact widths using quantum calculations. *Eur. Phys. J. D* **2011**, *61*, 285–290.
5. Seidel, J. Effects of ion motion on hydrogen Stark profiles. *Z. Naturforsch.* **1977**, *32a*, 1207–1214.
6. Duan, B.; Bari, M.A.; Wu, Z.Q.; Jun, Y.; Li, Y.M. Widths and shifts of spectral lines in He II ions produced by electron impact. *Phys. Rev. A* **2012**, *86*, 052502.
7. Griem, H.; Ralchenko, Y.V.; Bray, I. Stark broadening of the B III 2s-2p lines. *Phys. Rev. E* **1997**, *56*, 7186–7192.
8. Alexiou, S.; Lee, R.W. Semiclassical calculations of line broadening in plasmas: Comparison with quantal results. *J. Quant. Spectrosc. Radiat. Transf.* **2006**, *99*, 10–20.

9. Alexiou, S. *Phys. Rev. Lett.* Problem with the standard semiclassical impact line-broadening theory. **1995**, *75*, 3406–3409.
10. Alexiou, S.; ad Poquérusse, A. Standard line broadening impact theory for hydrogen including penetrating collisions. *Phys. Rev. E* **2005**, *72*, 046404.
11. Seaton, M.J. Line-profile parameters for 42 transitions in Li-like and Be-like ions. *J. Phys. B* **1988**, *21*, 3033–3054.
12. Ralchenko, Y.V.; Griem, H.; Bray, I.; Fursa, D.V. Electron collisional broadening of 2s3s-2s3p lines in Be-like ions. *J. Quant. Spectrosc. Radiat. Transf.* **2001**, *71*, 595–607.
13. Alexiou, S.; Lee, R.W.; Glenzer, S.; Castor, J. Analysis of discrepancies between quantal and semiclassical calculations of electron impact broadening in plasmas. *J. Quant. Spectrosc. Radiat. Transf.* **2000**, *65*, 15–22.
14. Elabidi, H.; Ben Nessib, N.; Cornille, M.; Dubau, J.; Sahal-Brechot, S. Electron impact broadening of spectral lines in Be-like ions: Quantum calculations. *J. Phys. B* **2008**, *41*, 025702.
15. Bouguettaia, H.; Chihi, Is.; Chenini, K.; Meftah, M.T.; Khelfaoui, F.; Stamm, R. Application of path integral formalism in spectral line broadening: Lyman- α in hydrogenic plasma. *J. Quant. Spectrosc. Radiat. Transf.* **2005**, *94*, 335-346.
16. Alexiou, S. Problems with the use of line shifts in plasmas. *J. Quant. Spectrosc. Radiat. Transf.* **2003**, *81*, 461-471.
17. Gunderson, M.A.; Haynes, D.A.; Kilcrease, D.P. Using semiclassical models for electron broadening and line shift calculations of $\Delta n=0$ and $\Delta n \neq 0$ dipole transitions. *J. Quant. Spectrosc. Radiat. Transf.* **2006**, *99*, 255–264.
18. Stambulchik, E.; Maron, Y. A study of ion-dynamics and correlation effects for spectral line broadening in plasma: K-shell lines. *J. Quant. Spectrosc. Radiat. Transf.* **2006**, *99*, 730–749.
19. Gigosos, M.A.; Cardenoso, V. New plasma diagnosis tables of hydrogen Stark broadening including ion dynamics. *J. Phys. B: Atomic, Mol. Opt. Phys.* **1996**, *29*, 4795-4838.
20. Sahal-Brechot, S. Impact theory of the broadening and shift of spectral lines due to electrons and ions in a plasma. *Astron. Astrophys.* **1969**, *1*, 91-123.
21. Sahal-Brechot, S. Impact theory of the broadening and shift of spectral lines due to electrons and ions in a plasma. *Astron. Astrophys.* **1969**, *2*, 322–354.
22. Sahal-Brechot, S. Stark broadening of isolated lines in the impact approximation, *Astron. Astrophys.* **1974**, *35*, 319–321.
23. Fleurier, C.; Sahal-Brechot, S.; Chapelle, J. Stark profiles of some ion lines of alkaline earth elements. *J. Quant. Spectrosc. Radiat. Transf.* **1977**, *17*, 595–604.
24. Dimitrijević, M.S.; Sahal-Brechot, S. Comparison of measured and calculated Stark broadening parameters for neutral-helium. *Phys. Rev. A* **1985**, *31*, 316–320.
25. Elabidi, H.; Sahal-Brechot, S.; Ben Nessib, N. Quantum Stark broadening of 3s-3p spectral lines in Li-like ions; Z-scaling and comparison with semi-classical perturbation theory. *Eur. Phys. J. D* **2009**, *54*, 51–64.
26. Stambulchik, E.; Alexiou, S.; Griem, H.R.; Kepple, P.C. Stark broadening of high principal quantum number hydrogen Balmer lines in low-density laboratory plasmas. *Phys. Rev. E* **2007**, *75*, 016401.

27. Gigosos, M.A.; Gonzalez, M.A.; Konjevic, N. On the Stark broadening of Sr+ and Ba+ resonance lines in ultracold neutral plasmas. *Eur. Phys. J. D* **2006**, *40*, 57–63.
28. Hegerfeldt, G.C.; Kesting, V. Collision-time simulation technique for pressure-broadened spectral lines with applications to Ly- α . *Phys. Rev. A* **1988**, *37*, 1488–1496.

© 2014 by the authors; licensee MDPI, Basel, Switzerland. This article is an open access article distributed under the terms and conditions of the Creative Commons Attribution license (<http://creativecommons.org/licenses/by/3.0/>).